Front. Phys. 13(4), 137108 (2018)
https://doi.org/10.1007/s11467-018-0813-z

RESEARCH ARTICLE

Electron mass enhancement and magnetic phase separation near the Mott transition in double-layer ruthenates

Jin Peng[1,†], X. M. Gu[2], G. T. Zhou[2], W. Wang[2], J. Y. Liu[3], Yu Wang[3], Z. Q. Mao[3], X. S. Wu[2], Shuai Dong[1]

[1] *School of Physics, Southeast University, Nanjing 211189, China*
[2] *Collaborative Innovation Center of Advanced Microstrucutres, Lab of Solid State Microstructures, School of Physics, Nanjing University, Nanjing 210093, China*
[3] *Department of Physics and Engineering Physics, Tulane University, New Orleans, LA 70118, USA*
Corresponding author. E-mail: [†]*jpeng@seu.edu.cn*
Received May 9, 2018; accepted June 19, 2018

We present a detailed investigation of the specific heat of $Ca_3(Ru_{1-x}M_x)_2O_7$ (M = Ti, Fe, Mn) single crystals. Depending on the dopant and doping level, three distinct regions are present: a quasi-two-dimensional metallic state with antiferromagnetic (AFM) order formed by ferromagnetic bilayers (AFM-b), a Mott insulating state with G-type AFM order (G-AFM), and a localized state with a mixed AFM-b and G-AFM phase. Our specific heat data provide deep insights into the Mott transitions induced by Ti and Mn doping. We observed not only an anomalous large mass enhancement, but also an additional term in the specific heat, i.e., $C \propto T^2$, in the localized region. The $C \propto T^2$ term is most likely due to long-wavelength excitations with both FM and AFM components. A decrease in the Debye temperature is observed in the G-type AFM region, indicating lattice softening associated with the Mott transition.

Keywords specific heat, ruthenates, Mott insulator, phase separation

PACS numbers 71.30+h, 75.50Ee, 75.40.Cx

1 Introduction

The insulator–metal transition (IMT), accompanied by a huge resistivity change, is one of the most studied phenomena in condensed matter physics [1, 2]. It not only has promising applications in next-generation information technology, but is also fundamentally important for studying the underlying physics of correlated electronic systems [3, 4]. Interestingly, although there are many observations of IMTs upon tuning of the one-electron bandwidth W or band filling by doping, there are few reports on Mott transitions driven by adding impurities to a metal at low concentrations. One example of such an impurity-induced Mott transition is found in the prototype system V_2O_3 [5]. As V^{3+} is replaced by Ti^{3+}, the system becomes metallic. However, if V^{3+} is replaced by Cr^{3+} instead, the Mott insulating phase is enhanced [6]. Castellani *et al.* proposed that each Cr^{3+} ion acts as a strong scattering center; thus, increasing the Cr^{3+} content results in an increase in the nonpolar state weight with respect to the polar state weight, ultimately leading to non-conductivity [7]. This type of transition should be a type of percolation problem. The IMT described above, and its related metal–insulator transition (MIT), have high technological potential for use in, among other applications, intelligent windows and field-effect transistors. Later experimental efforts did support the view of phase separation near the Mott transition in this system. Another puzzling phenomenon observed in the system is an anomalous metallic state in which the specific-heat coefficient γ near the MIT shows strong enhancement [8].

In this paper, we present another system that shows an impurity-induced Mott insulating state, the Ruddlesden–Popper-type layered ruthenates $(Sr, Ca)_{n+1}Ru_nO_{3n+1}$ [9]. This system exhibits various ground states, including spin-triplet superconductivity (Sr_2RuO_4) [10, 11], an enhanced paramagnetic (PM) metallic state ($Sr_3Ru_2O_7$) [12], itinerant ferromagnetism ($SrRuO_3$) [13], an antiferromagnetic (AFM) Mott insulating state (Ca_2RuO_4) [14, 15], a quasi-two-dimensional (quasi-2D) metallic

*arXiv: 1807.01991.

state with AFM order ($Ca_3Ru_2O_7$) [16, 17], and a PM "bad" metallic state ($CaRuO_3$) [18]. Our previous study showed that although the ground states are diverse, the doping effects of some 3*d* ions on the Ru sites are consistent. That is, Mn and Ti dopants induce or enhance the Mott insulating state and AFM coupling, whereas Cr, Fe, and Co enhance the FM coupling [19]. For example, the double-layer ruthenate $Ca_3Ru_2O_7$ shows an AFM transition at 56 K, followed by an MIT at 48 K [20]. The in-plane resistivity recovers to the metallic state below 30 K [16]. The AFM state below 56 K is characterized by FM bilayers coupled antiferromagnetically along the *c* axis. The spin direction switches from the *a* axis (AFM-a) for $T_{\rm MIT} < T < T_{\rm N}$ to the *b* axis (AFM-b) for $T < T_{\rm MIT}$ [17, 21]. As little as 3% Ti doping or 4% Mn doping on the ruthenium site can tune the system from a quasi-2D metallic state with AFM-b order to a Mott insulating state with G-type AFM order through a phase separation region [19, 22, 23]. However, Fe doping on the ruthenium site will not lead to a Mott insulating state; instead, the system shows a localized electronic state with coexisting AFM-b and incommensurate magnetic (ICM) structure [24]. A detailed phase diagram is shown in Fig. 1. A schematic diagram of the three magnetic structures, AFM-b, G-AFM, and ICM, is shown in Fig. 4. Here, we report on the nature of this impurity-induced Mott transition as revealed by specific heat measurements, including the phase separation and anomalous metallic state.

2 Experimental details

Single-crystal samples were grown by floating zone methods. All the samples used in our experiments were examined by X-ray diffraction (XRD) measurements and

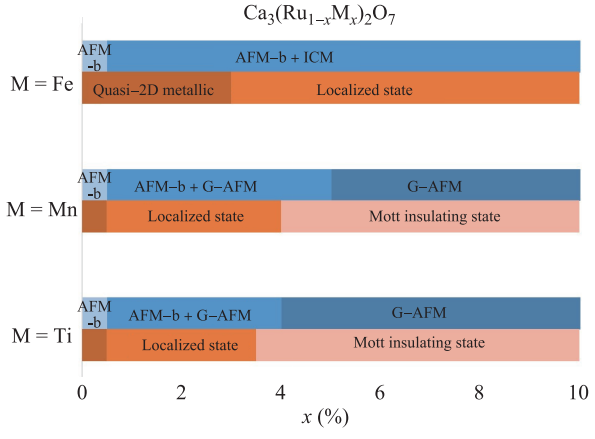

Fig. 1 Magnetic and electronic phase diagram of $Ca_3(Ru_{1-x}M_x)_2O_7$ (M = Ti, Fe, Mn), magnetic and electronic states are represented by different colored region and labeled.

proven to be composed of a pure bilayered phase. Successful doping of Ti, Mn, and Fe ions into the single crystals was confirmed by energy-dispersive X-ray spectroscopy. The observed compositions are generally consistent with the nominal ones. The chemical formula given here indicates the observed composition. Heat capacity measurements at 2–200 K were made in a physical property measurement system (Quantum Design) using relaxation measurements. The masses of the samples were measured by a thermogravimetric analysis system with an accuracy of 0.01 mg.

3 Results and discussion

The global temperature dependence of the specific heat *C* of Mn-doped $Ca_3Ru_2O_7$ is shown in Fig. 2(a). The most notable high-*T* features are the peaks at the magnetic ordering temperature T_N and the MIT temperature T_{MIT}. The parent compound, $Ca_3Ru_2O_7$, is ordered antiferromagnetically at $T_N = 56$ K, and an MIT occurs at 48 K. A broad "ambda anomaly"s observed at T_N; a sharp peak is observed at T_{MIT}. These results indicate that the magnetic transition from PM to AFM-a is of second order, and the MIT associated with the magnetic transition from AFM-a to AFM-b is of first order. When the Mn dopant is introduced, the peak corresponding to the MIT first moves to a lower temperature and splits into two small peaks (1% Mn, 2% Mn); it then gradually emerges as a bump (3% Mn, 4% Mn). In addition, the broad "ambda anomaly" orresponding to the AFM order is scarcely affected by the Mn dopant. When the Mn doping level exceeds 5%, the MIT and magnetic transition merge, leaving only one sharp peak at a dramatically higher temperature. This is seen more clearly by subtracting the smooth background using a high-order polynomial function [Fig. 2(b)]. Ti-doped samples exhibit behavior similar to that of Mn-doped ones, as shown in Fig. 2(c), except that the critical concentration is 4% instead of 5%. For Fe-doped samples, the "ambda anomaly"oves to higher temperature, and the MIT moves to lower temperature more efficiently than in the Mn- and Ti-doped samples. T_N reaches $\sim$ 80 K at only the 5% doping level. Further, the MIT and magnetic ordering never merge until the highest doping level that was successfully synthesized.

The observations in Fig. 2 clearly reveal three distinct composition groups for the 3*d* doped $Ca_3Ru_2O_7$ system. Group 1 is the parent compound, which is characterized by a "ambda anomaly"nd a sharp peak, separates the compound into a high-temperature PM phase, medium-temperature AFM-a phase, and low-temperature AFM-b phase. Group 2 contains the samples doped with Ti or Mn at low concentrations and all the Fe-doped samples.

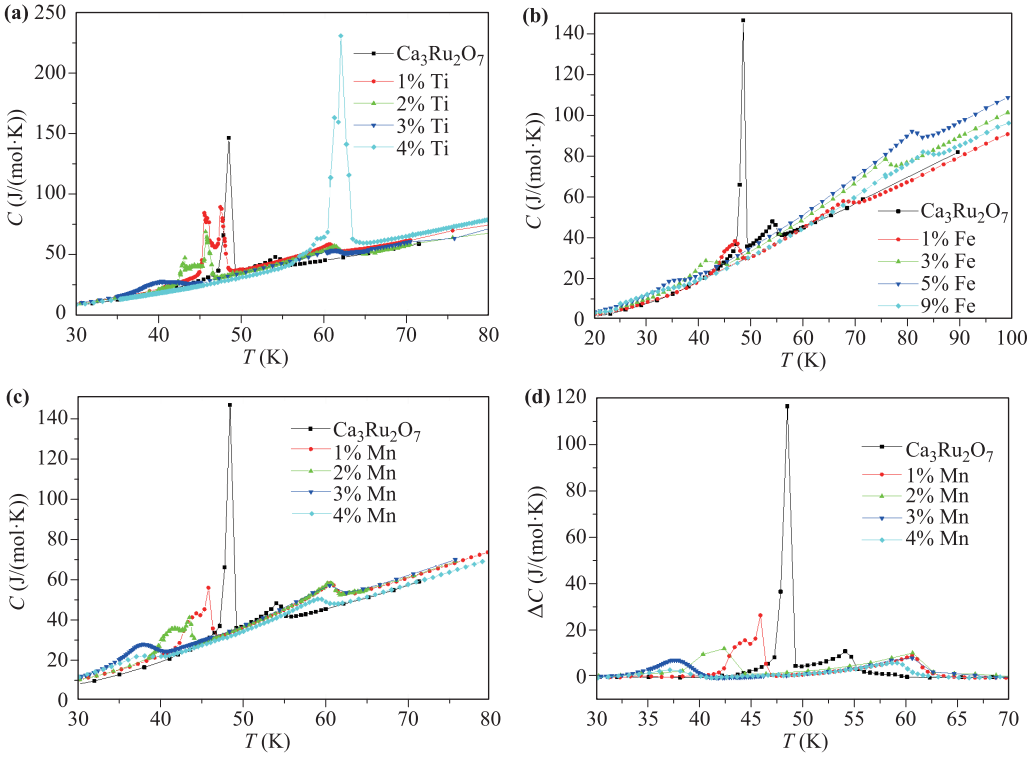

Fig. 2 Temperature dependence of the specific heat of: **(a)** pure, 1% Ti, 2% Ti, 3% Ti and 4% Ti doped $Ca_3Ru_2O_7$ (30 K–80 K); **(b)** pure, 1% Fe, 3% Fe, 5% Fe and 9% Fe doped $Ca_3Ru_2O_7$ (30–80 K); **(c)** pure, 1% Mn, 2% Mn, 3% Mn and 4% Mn doped $Ca_3Ru_2O_7$ (30–80 K); **(d)** Excess (magnetic) specific heat extracted from the data in (c) by subtracting a smooth background as described in the text.

An intermediate magnetic phase emerges between AFM-a and AFM-b. This intermediate phase was characterized carefully by elastic neutron scattering measurements and was found to consist of coexisting commensurate and incommensurate phases. In group 3, which consists of the samples with high-concentration Ti or Mn doping, a single strong peak separates the high-temperature PM metallic phase and low-temperature G-AFM Mott insulating state. We will further discuss these regions in detail by analyzing the low-temperature specific heat.

The low-temperature region (2 K $< T <$ 10 K) is shown in Fig. 3 for selected compositions. The data are plotted as C/T vs. T^2 and can be divided into the contributions from different excitations as follows: $C = C_V + C_e + C_M + C_h$, where C_V is the lattice contribution, which is equal to βT^3, and β is given in the Debye model by $\beta = 234Nk_B/\theta_D^3$. We found that it is not necessary to add a T^5 term to the lattice contribution C_V to achieve an adequate fit. C_e is the electron contribution, which is equal to γT; the Sommerfeld coefficient γ is given by $\gamma = \pi^2 k_B^2 N(E_F)/3$, where $N(E_F)$ is the density of states at the Fermi level. The compositions in group 1 ($Ca_3Ru_2O_7$) and group 3 (10% Ti and 8% Mn) can be simply fitted using only these two factors, $C = \gamma T + \beta T^3$, as shown by the red curves in Fig. 3.

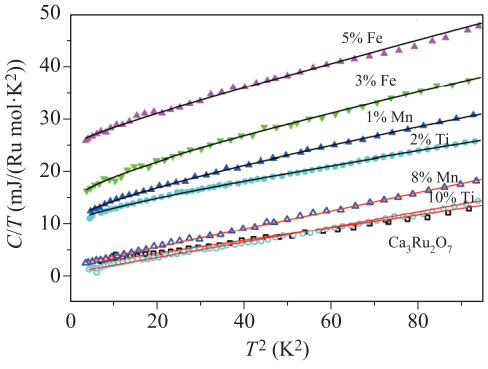

Fig. 3 Temperature dependence of the specific heat (2–10 K) of 7 compositions (5% Fe, 3% Fe, 1% Mn, 2% Ti, 8% Mn, 10% Ti and $Ca_3Ru_2O_7$) plotted as C/T vs. T^2. The solid lines are fitted to $C = \gamma T + BT^2 + \beta T^3$, a model that is described in detail in text. The Adj. R-square parameters for these fittings are 0.98215, 0.99773, 0.99933, 0.99819, 0.99873, 0.99179, and 0.9876, respectively.

However, the compositions in group 2 (1% Mn, 2% Ti, 3% Fe, and 5% Fe) show an obvious downward turn at the low-temperature limit, indicating a lower-order term than βT^3. The data for these compositions are thus fitted to $C = \gamma T + BT^2 + \beta T^3$. The parameters γ and B

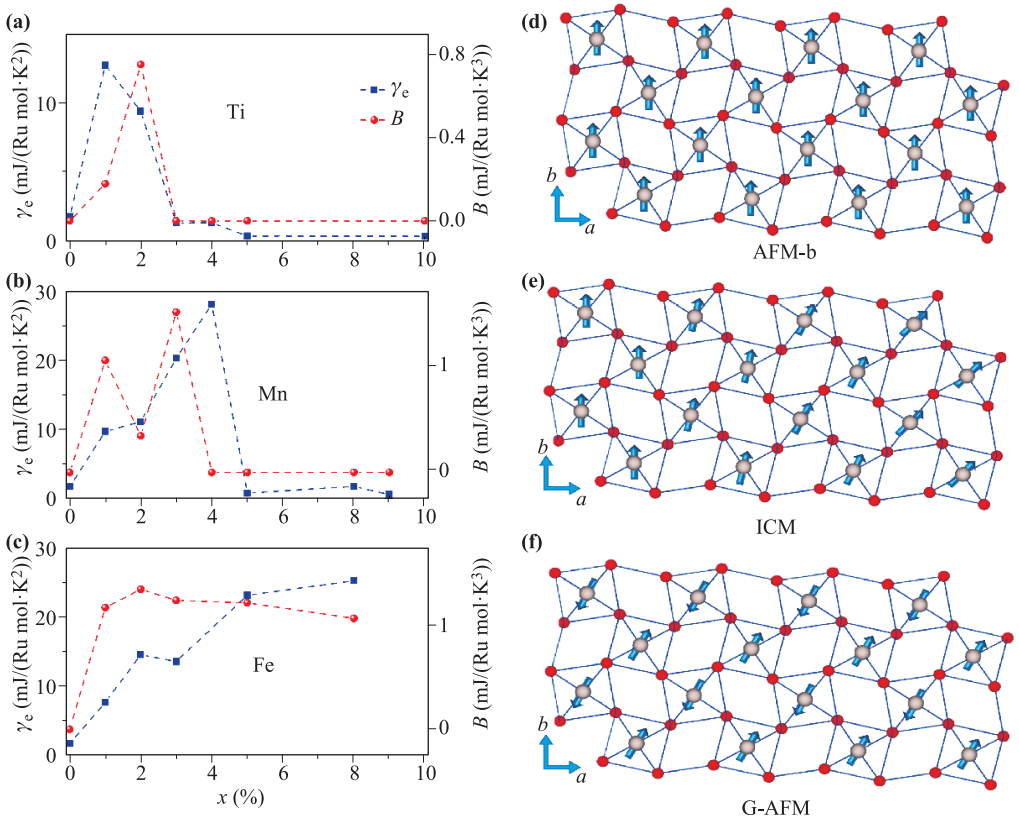

Fig. 4 Doping dependence of Sommerfeld coefficient γ and T^2 contribution B to the specific heat for Ti **(a)**, Mn **(b)** and Fe **(c)** doped $Ca_3Ru_2O_7$. **(d)** In-plane view of AFM-b magnetic strcuture. **(e)** In-plane view of incommensurate magnetic structure. **(f)** In-plane view of G-AFM magnetic structure.

are summarized in Fig. 4. The Debye temperature θ_D derived from the parameter β is plotted as a function of doping level in Fig. 5.

The T^2 contribution to the specific heat has been observed in the manganite $La_{1-x}Sr_xMnO_{3+\delta}$ when it is an A-type antiferromagnet [25]. For a model with linear dispersion for the planar FM excitation and quadratic dispersion for the linear AFM excitation, the combined dispersion relationship yields the low-temperature magnetic contribution to the specific heat, offering a plausible candidate for the T^2 term. However, this interpretation cannot be directly applied to our system. First, the proposed model is that of a three-dimensional infinite-layer perovskite structure (ABO_3 type). The system studied here is a quasi-2D double-layer perovskite structure. AFM-b consists of FM double layers coupled antiferromagnetically along the c axis. The magnetic excitations include not only planar FM and linear AFM, but also linear FM excitation. Thus, the dispersion relationships will differ from those of the A-type AFM structure. Second, the T^2 term was not observed in the parent compound $Ca_3Ru_2O_7$, which also showed the AFM-b ground state.

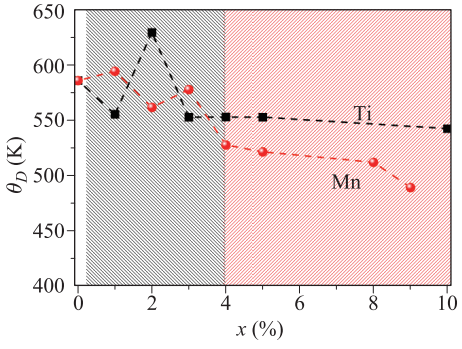

Fig. 5 Doping dependence of the Debye temperature θ_D for Mn and Ti doped $Ca_3Ru_2O_7$.

We further found that other compounds that do not have A-type AFM structure also have a T^2 term, for example, electron-doped $CaMnO_3$ and $La_{1-x}Sr_xCoO_3$ [26, 27]. It was attributed to long-wavelength excitations with both FM and AFM components due to the magnetic phase separation. This seems similar to our situation. In the group 2 compositions, the ground states of the Mn- and Ti-doped compounds produce the phase separation between the AFM-b and G-type AFM states. The Fe-doped samples consist of both a commensurate AFM-b phase and an incommensurate phase formed of a cycloidal spiral spin structure. Regrettably, theoretical

studies of the magnetic entities are still lacking.

Another puzzling feature is the strong enhancement of the Sommerfeld coefficient γ in the group 2 compositions. The in-plane transport behavior of the group 2 samples shows an insulating/semiconducting temperature dependence with low residual resistivity. We named this region the localized state, in contrast to the Mott insulating state of the group 3 compositions. Usually γ can be expressed as $\gamma = (\pi^2/3)k_B^2 n(\varepsilon_F)$, where k_B is the Boltzmann constant, and $n(\varepsilon_F)$ is the density of states (DOS) at the Fermi level, ε_F. Therefore, γ is a linear function of $n(\varepsilon_F)$. However, various experiments reported a finite value of γ in insulating materials such as vitreous silica, germania, and selenium. Subsequently, it was proposed that in insulating materials, charge carriers can tunnel through the potential barriers between various local minima. The energy difference between the local minima will vary continuously in an amorphous system, which leads to a linear term in the specific heat. Interestingly, various studies of manganites reveal a large γ in insulating crystalline compositions. For example, the electron-doped system $La_{2.3}Ca_{0.7}Mn_2O_7$ was found to have $\gamma = 41$ mJ/(mol·K^2), and in $Nd_{0.67}Sr_{0.33}MnO_3$, a value of $\gamma = 25$ mJ/(mol·K^2) was observed [28, 29]. In hole-doped $LaMnO_{3+\delta}$, γ is as high as 23 mJ/(mol·K^2) [30]. To explain such anomalous observations, various scenarios have been proposed. It was suggested that the DOS at ε_F is finite but localized, which gives rise to finite γ and insulating transport. The other suggestion is that a spin glass phase is possible.

In undoped $Ca_3Ru_2O_7$, the small value of the Sommerfeld coefficient [$\gamma \sim 1.7$ mJ/(Ru mol·K^2)] arising from the non-nesting Fermi surface pockets survived. In Ru-site-doped $Ca_3Ru_2O_7$, the itinerant Ru t_{2g} electrons may be localized owing to the potential fluctuations arising from cation substitution and spin-dependent fluctuations due to local deviations from AFM-b magnetic order. If the doping concentration is fairly low, the localization length may be fairly large. Charge carriers can thus hop through a number of Ru ions, defines limited length of bilayer FM clusters. On the other hand, the electron levels, although localized, are not widely spaced in energy, allowing for thermal excitation that contributes a linear term to the specific heat. From Fig. 4, we noticed that enhanced the γ appears simultaneously with the T^2 term. As stated above, the T^2 term is due to long-wavelength excitations with both FM and AFM components in the magnetic phase separation region. The scenario proposed above is consistent with this picture.

The above scenario explains the nonzero Sommerfeld coefficient of the insulating state and why this coefficient is one order larger than that of the pristine compound. In fact, enhanced γ near a Mott transition is ubiquitous, especially in materials with antiferromagnetism, for example, heavy fermion compounds, high-T_c cuprates, and the Mott–Hubbard systems V_2O_3 and $Ni(Se_{1-x}S_x)_2$ [8, 31, 32]. In the V_2O_3 system, a metallic state can be achieved by Ti doping, applied pressure, or V deficiency upon tuning of the one-electron bandwidth W or band filling by doping. In the former route (tuning of the one-electron bandwidth W), the electronic effective mass m^* diverges at the MIT with a negligible change in carrier concentration. For the latter route (band filling by doping), m^* actually decreases as the MIT approaches. Our case is obviously closer to the former route. The mechanism of mass enhancement can be magnetic polarons, lattice polarons, Coulomb interaction effects, or Van Hove singularities near the Fermi level.

In addition, we found that the Sommerfeld coefficient γ and the T^2 contribution B are enhanced simultaneously in the group 2 region, as shown in Fig. 4. As stated above, the enhancement of the Sommerfeld coefficient γ was due to tunneling of charge carriers through the potential barriers between various local minima. The T^2 contribution B is not attributed to long-wavelength excitations with both FM and AFM components. The coexistence of FM and AFM components can be explained by competition between the double-exchange FM interaction and superexchange interactions. The double-exchange FM interaction is mediated via Hund's rule coupling between itinerant electrons and localized moments. An FM state occurs when the system has sufficient itinerant carriers. In contrast, superexchange does not involve real carrier transfer. It applies mainly to the localized state. In this scenario, both FM and AFM exchange can occur depending on the orbital occupancy according to the Goodenough–Kanamori rule. If only superexchange is considered, on the basis of the Goodenough–Kanamori rule, the Ru^{4+}–Ru^{4+} coupling should be AFM. Therefore, the coexistence of FM and AFM components indicates that some itinerant electrons remain in the group 2 region, which also explains the nonzero Sommerfeld coefficient γ.

If the Mn or Ti doping level is further increased to the group 3 compositions, both the T^2 term and the Sommerfeld coefficient γ become negligible. This is understandable because the ground states of this group's samples are the G-type AFM Mott insulating state. For G-type antiferromagnetism, the magnetic excitation contributes a T^3 term to the heat capacity. This will result in overestimation of the Debye temperature θ_D derived using the parameter β. Considering θ_D, we first see that the overall magnitude of 450–650 K is typical of perovskite oxides of this type and consistent with the values for other Ruddlesden–Popper-type ruthenates. The most surprising feature is the obvious reduction of θ_D in the G-type AFM region, especially considering that θ_D has already been overestimated in this group. This reduc-

tion suggests a significant change in the lattice dynamics across the Mott transition. It is natural to correlate this with the known discontinuity in the unit cell parameters. For compositions in the third group, the lattices are significantly flattened compared to those of compounds in groups 1 and 2 from XRD and neutron measurements. A reduction in θ_D is also observed in $La_{1-x}Sr_xMnO_3$ single crystals, where it was interpreted in terms of lattice softening induced by dynamical short-range Jahn–Teller distortions [33]. Such distortions could also play a key role in this system.

4 Conclusion

In summary, we performed a comprehensive study of the heat capacity of the Ru-site-doped $Ca_3Ru_2O_7$ system and found that all the compositions can be divided into three groups. We observed two conventional contributions to the heat capacity at low T, a lattice contribution ($\propto T^3$) and an electronic contribution ($\propto T$), in addition to an unexpected T^2 contribution in the group 2 compositions. The doping dependence of the parameters of these terms was analyzed in detail and yielded a significant amount of information on the impurity-induced Mott transition. In particular, we found evidence for the percolation nature of the Mott transition and a large electron mass enhancement due to strong electron–electron correlations in the localized state. Additionally, we also found lattice softening in the Mott insulating state. The doping dependence of the T^2 contribution and electronic contribution ($\propto T$) was shown to provide a detailed picture of the evolution of the phase-separated state upon doping. These results not only clarify the systematics of the magnetic phase separation in this system; they also emphasize the usefulness of specific heat measurements as a powerful probe of magnetic inhomogeneity.

Acknowledgements We gratefully acknowledge financial support from the Fundenmental Research Funds for the Central Universities China (No. 3207028403). Work at Nanjing University was supported by the National key R&D program of China (Grant No. 2017YFA0303202). The sample growth and high-temperature specific heat measurements at Tulane University were supported by the U. S. Department of Energy under EPSCOR Grant No. DE-SC0012432 with additional support from the Louisiana Board of Regents.

References

1. M. Imada, A. Fujimori, and Y. Tokura, Metal-insulator transitions, *Rev. Mod. Phys.* 70(4), 1039 (1998)
2. V. R. Shaginyan, A. Z. Msezane, G. S. Japaridze, K. G. Popov, and V. A. Khodel, Strongly correlated Fermi systems as a new state of matter, *Front. Phys.* 11(5), 117103 (2016)
3. L. F. Lin, L. Z. Wu, and S. Dong, Interfacial phase competition induced Kondo-like effect in manganite-insulator composites, *Front. Phys.* 11(6), 117502 (2016)
4. Y. Xing, Y. Sun, M. Singh, Y. F. Zhao, M. H. W. Chan, and J. Wang, Electronic transport properties of topological insulator films and low dimensional superconductors, *Front. Phys.* 8(5), 491 (2013)
5. P. D. Dernier and M. Marezio, Crystal structure of the low-temperature antiferromagnetic phase of V_2O_3, *Phys. Rev. B* 2(9), 3771 (1970)
6. D. B. McWhan, A. Menth, J. P. Remeika, W. F. Brinkman, and T. M. Rice, Metal-insulator transitions in pure and doped V_2O_3, *Phys. Rev. B* 7(5), 1920 (1973)
7. C. Castellani, C. R. Natoli, and J. Ranninger, Metal-insulator transition in pure and Cr-doped V_2O_3, *Phys. Rev. B* 18(9), 5001 (1978)
8. S. A. Carter, T. F. Rosenbaum, P. Metcalf, J. M. Honig, and J. Spalek, Mass enhancement and magnetic order at the Mott–Hubbard transition, *Phys. Rev. B* 48(22), 16841 (1993)
9. S. N. Ruddlesden and P. Popper, New compounds of the K_2NIF_4 type, *Acta Crystallogr.* 10(8), 538 (1957)
10. Y. Maeno, H. Hashimoto, K. Yoshida, S. Nishizaki, T. Fujita, J. G. Bednorz, and F. Lichtenberg, Superconductivity in a layered perovskite without copper, *Nature* 372(6506), 532 (1994)
11. K. Ishida, H. Mukuda, Y. Kitaoka, K. Asayama, Z. Q. Mao, Y. Mori, and Y. Maeno, Spin-triplet superconductivity in Sr_2RuO_4 identified by ^{17}O Knight shift, *Nature* 396(6712), 658 (1998)
12. S. A. Grigera, R. S. Perry, A. J. Schofield, M. Chiao, S. R. Julian, G. G. Lonzarich, S. I. Ikeda, Y. Maeno, A. J. Millis, and A. P. Mackenzie, Magnetic field-tuned quantum criticality in the metallic ruthenate $Sr_3Ru_2O_7$, *Science* 294(5541), 329 (2001)
13. J. M. Longo, P. M. Raccah, and J. B. Goodenough, Magnetic Properties of $SrRuO_3$ and $CaRuO_3$, *J. Appl. Phys.* 39(2), 1327 (1968)
14. S. Nakatsuji, S. I. Ikeda, and Y. Maeno, Ca_2RuO_4: New Mott insulators of layered ruthenate, *J. Phys. Soc. Jpn.* 66(7), 1868 (1997)
15. J. H. Jung, Z. Fang, J. P. He, Y. Kaneko, Y. Okimoto, and Y. Tokura, Change of electronic structure in Ca_2RuO_4 induced by orbital ordering, *Phys. Rev. Lett.* 91(5), 056403 (2003)
16. Y. Yoshida, I. Nagai, S. I. Ikeda, N. Shirakawa, M. Kosaka, and N. Môri, Quasi-two-dimensional metallic ground state of $Ca_3Ru_2O_7$, *Phys. Rev. B* 69(22), 220411 (2004)

17. Y. Yoshida, S. I. Ikeda, H. Matsuhata, N. Shirakawa, C. H. Lee, and S. Katano, Crystal and magnetic structure of $Ca_3Ru_2O_7$, *Phys. Rev. B* 72(5), 054412 (2005)
18. K. Yoshimura, T. Imai, T. Kiyama, K. R. Thurber, A. W. Hunt, and K. Kosuge, O^{17} NMR observation of universal behavior of ferromagnetic spin fluctuations in the itinerant magnetic system $Sr_{1-x}Ca_xRuO_3$, *Phys. Rev. Lett.* 83(21), 4397 (1999)
19. J. Peng, M. Q. Gu, X. M. Gu, G. T. Zhou, X. Y. Gao, J. Y. Liu, W. F. Xu, G. Q. Liu, X. Ke, L. Zhang, H. Han, Z. Qu, D. W. Fu, H. L. Cai, F. M. Zhang, Z. Q. Mao, and X. S. Wu, Mott transition controlled by lattice-orbital coupling in 3 d -metal-doped double-layer ruthenates, *Phys. Rev. B* 96(20), 205105 (2017)
20. G. Cao, S. McCall, J. E. Crow, and R. P. Guertin, Observation of a metallic antiferromagnetic phase and metal to nonmetal transition in $Ca_3Ru_2O_7$, *Phys. Rev. Lett.* 78(9), 1751 (1997)
21. W. Bao, Z. Q. Mao, Z. Qu, and J. W. Lynn, Spin valve effect and magnetoresistivity in single crystalline $Ca_3Ru_2O_7$, *Phys. Rev. Lett.* 100(24), 247203 (2008)
22. X. Ke, J. Peng, D. J. Singh, T. Hong, W. Tian, C. R. Dela Cruz, and Z. Q. Mao, Emergent electronic and magnetic state in $Ca_3Ru_2O_7$ induced by Ti doping, *Phys. Rev. B* 84(20), 201102 (2011)
23. J. Peng, X. Ke, G. Wang, J. E. Ortmann, D. Fobes, T. Hong, W. Tian, X. Wu, and Z. Q. Mao, From quasi-two-dimensional metal with ferromagnetic bilayers to Mott insulator with G-type antiferromagnetic order in $Ca_3(Ru_{1-x}Ti_x)_2O_7$, *Phys. Rev. B* 87(8), 085125 (2013)
24. X. Ke, J. Peng, W. Tian, T. Hong, M. Zhu, and Z. Q. Mao, Commensurate-incommensurate magnetic phase transition in the Fe-doped bilayer ruthenate $Ca_3Ru_2O_7$, *Phys. Rev. B* 89(22), 220407 (2014)
25. B. F. Woodfield, M. L. Wilson, and J. M. Byers, Low-temperature specific heat of $La_{1-x}Sr_xMnO_{3+d}$, *Phys. Rev. Lett.* 78(16), 3201 (1997)
26. A. L. Cornelius, B. E. Light, and J. J. Neumeier, Evolution of the magnetic ground state in the electron-doped antiferromagnet $CaMnO_3$, *Phys. Rev. B* 68(1), 014403 (2003)
27. C. He, S. Eisenberg, C. Jan, H. Zheng, J. F. Mitchell, and C. Leighton, Heat capacity study of magnetoelectronic phase separation in $La_{1-x}Sr_xCoO_3$ single crystals, *Phys. Rev. B* 80(21), 214411 (2009)
28. P. Raychaudhuri, C. Mitra, A. Paramekanti, R. Pinto, A. K. Nigam, and S. K. Dhar, The metal-insulator transition and ferromagnetism in the electron-doped layered manganites ($x = 0, 0.3, 0.5$), *J. Phys. Condens. Matter* 10(12), L191 (1998)
29. J. E. Gordon, R. A. Fisher, Y. X. Jia, N. E. Phillips, S. F. Reklis, D. A. Wright, and A. Zettl, Specific heat of $Nd_{0.67}Sr_{0.33}MnO_3$, *Phys. Rev. B* 59(1), 127 (1999)
30. L. Ghivelder, I. Abrego Castillo, M. A. Gusmão, J. A. Alonso, and L. F. Cohen, Specific heat and magnetic order in $LaMnO_{3+d}$, *Phys. Rev. B* 60(17), 12184 (1999)
31. K. Mamiya, T. Mizokawa, A. Fujimori, T. Miyadai, N. Chandrasekharan, S. R. Krishnakumar, D. D. Sarma, H. Takahashi, N. Môri, and S. Suga, Photoemission study of the metal-insulator transition in $NiS_{2-x}Se_x$, *Phys. Rev. B* 58(15), 9611 (1998)
32. S. Ogawa, Magnetic properties of 3d transition-metal dichalcogenides with the pyrite structure, *J. Appl. Phys.* 50(B3), 2308 (1979)
33. T. Okuda, A. Asamitsu, Y. Tomioka, T. Kimura, Y. Taguchi, and Y. Tokura, Critical behavior of the metal-insulator transition in $La_{1-x}Sr_xMnO_3$, *Phys. Rev. Lett.* 81(15), 3203 (1998)